Quantum transport in quasiperiodic lattice systems in the presence of Büttiker probes

Madhumita Saha,[1,*] B. Prasanna Venkatesh,[2,†] and Bijay Kumar Agarwalla[1,‡]
[1]*Department of Physics, Indian Institute of Science Education and Research Pune, Dr. Homi Bhabha Road, Ward No. 8, NCL Colony, Pashan, Pune, Maharashtra 411008, India*
[2]*Department of Physics, Indian Institute of Technology Gandhinagar, Palaj, Gujarat 382355, India*

(Received 28 March 2022; accepted 1 June 2022; published 15 June 2022)

Quasiperiodic lattice systems offer diverse transport properties. In this paper, we investigate environment-induced effects on the transport properties for quasiperiodic systems, namely the one-dimensional Aubry-André-Harper (AAH) lattice chain and its generalized version (GAAH), by considering the Büttiker probe approach. We first consider a voltage-probe situation and study the electrical conductance properties in the linear-response regime. At zero temperature, we observe an enhancement in conductance for small probe coupling strength γ with a power-law scaling γ^4 at all the no-transport regimes, located both inside and outside of the band of the original system. For large probe coupling strengths, the conductance at all Fermi energies is the same and decays as a power law with scaling $1/\gamma^4$. This particular scaling survives even in the finite-temperature limit. Interestingly, this scaling result is different from the one recently predicted following the local Lindblad master equation approach. The transport eventually becomes diffusive for all energy ranges and in all regimes of the original model for a sufficiently strong coupling with the probes. We further extend our study and consider voltage-temperature probes to analyze the thermoelectric performance of the chain in terms of the figure of merit. We also demonstrate the validity of two recently obtained bounds on thermoelectric efficiency which are tighter than the seminal Carnot bound, in the presence of voltage-temperature probes.

DOI: 10.1103/PhysRevB.105.224204

I. INTRODUCTION

Quasiperiodic lattice systems reside between a completely disordered system and a periodically ordered system. Such systems can offer a lot of interesting and intriguing transport properties even in low dimensions [1–7]. Recent remarkable experimental realizations of quasiperiodic systems in various cold atom platforms [8–16] have triggered intense theoretical research activities to understand the underlying dynamical and steady-state transport properties. Moreover, some new studies in this context have further revealed the potential for realizing highly efficient quantum devices such as quantum rectifiers and thermoelectric engines by carefully exploiting the exotic transport properties [17–20].

The popular quasiperiodic lattice systems, namely, the Aubry-André-Harper (AAH), its generalized version GAAH model, and the Fibonacci model [5,21], have been studied extensively in the context of boundary driven dissipative quantum transport [22–29]. Further studies have started to emerge to understand the environment-induced effects on transport [30–39] in such systems. Very recently, following the local Lindblad master equation formalism, the steady-state transport properties due to dephasing noise were analyzed for AAH and Fibonacci models [34]. Following a similar approach, the effect of dephasing noise on transport was studied in the presence of a mobility edge [35]. Apart from this approach, another popular way to incorporate environment effects is the Büttiker probe technique. Such a technique is used extensively to understand effective many-body transport properties in setups such as molecular junctions [40–47], quantum dots [48], lattice models of oscillators, spins, fermions, excitons [37,49–51], etc. Very recently the authors in Ref. [36] extended the Büttiker probe approach to analyze the thermoelectric transport properties in Fibonacci-type quasiperiodic models [52–55] and pointed out that environment-induced processes can lead to a better thermoelectric performance in certain regimes of transport. However, a clear understanding of the transport and thermoelectric properties for other types of quasiperiodic systems such as the AAH and the GAAH model (quasiperiodic systems with a single-particle mobility edge) following the Büttiker probe approach is still missing.

In this paper, we therefore analyze how the transport properties in AAH and GAAH lattice models get modified in the presence of Büttiker probes. We implement both the voltage-probe and voltage-temperature probe techniques and explore electrical conductance and thermoelectric heat-to-work conversion properties in the linear-response regime. We point out the consequences for the conductance in both zero- and finite-temperature limits. We observe that in the presence of both the voltage and the voltage-temperature probes, the linear transport coefficients, namely the electrical and the thermal conductances, display a universal power-law decay with the probe coupling strength in the strong probe coupling regime. We provide a rigorous analytical proof for this result. Importantly, this universal behavior is different from the

*madhumita.saha@acads.iiserpune.ac.in
†prasanna.b@iitgn.ac.in
‡bijay@iiserpune.ac.in

behavior predicted following the local Lindblad master equation formalism, thus pinpointing crucial differences between the two approaches in mimicking the underlying many-body scattering processes. Furthermore, in the zero-temperature voltage-probe case, we observe environment-assisted transport for all the exponentially decaying regimes with a particular power-law scaling with probe strength. For the thermoelectric setup, we further assess and compare the recently obtained tighter bounds on efficiency following the thermodynamic uncertainty relations [56] and the bound obtained in Ref. [57].

We organize the paper as follows: In Sec. II, we introduce the AAH and the GAAH lattice models and then briefly describe the theoretical aspects of the Büttiker probe approach and how to obtain charge conductance in the linear-response regime. In Sec. III, we present the numerical results both in the zero- and finite-temperature limit. In Sec. IV, we extend our study to voltage-temperature probes and study the thermoelectric performance for the AAH chain and furthermore assess the recently obtained tighter bounds on efficiency by expressing these bounds in terms of the Onsager's transport coefficients. Finally, in Sec. V, we provide a summary highlighting our key findings. In the Appendix, we present a rigorous derivation and show the emergence of diffusive behavior for conductance as well as its scaling with the probe coupling strength in the strong probe coupling limit.

II. MODEL AND THEORY

A. Model Hamiltonian

We consider an out-of-equilibrium one-dimensional quasiperiodic lattice chain that is connected at its two ends to two thermochemical reservoirs. These reservoirs are always maintained at fixed chemical potentials and temperatures. Since we are interested in investigating the environment-induced effects on the central quasiperiodic lattice chain, we connect uniform and independent local reservoirs, i.e., Büttiker probes, to each lattice site. The Hamiltonian for the entire setup is then given as

$$H = H_S + H_B + H_{SB} + H_P + H_{PS}, \tag{1}$$

where H_S represents a quasiperiodic chain with a Hamiltonian

$$H_S = \sum_i \epsilon_i c_i^\dagger c_i + t \sum_i (c_{i+1}^\dagger c_i + c_i^\dagger c_{i+1}). \tag{2}$$

Here, $c_i^\dagger$ (c_i) is the creation (annihilation) operator for the electron at the i th site. Here, we consider only the nearest-neighbor hopping with hopping amplitude t. The site-dependent on-site potential ϵ_i mimics a quasiperiodic potential which for the generalized Aubry-André-Harper (GAAH) model is given as

$$\epsilon_i = \frac{2\lambda \cos[2\pi bi + \Phi]}{1 + \alpha \cos[2\pi bi + \Phi]}, \tag{3}$$

where λ represents the strength of the potential, b is an irrational number which makes the potential quasiperiodic, and Φ is the phase factor that generates different configurations of the quasiperiodic potential. For, $\alpha = 0$, this model reduces to the AAH model [1,2]. For the AAH model, all the single-particle eigenstates are delocalized for $\lambda < 1$ and exponentially localized for $\lambda > 1$ [1] and at $\lambda = 1$ all the states are critical, i.e., neither localized nor delocalized. As a result, the particle transport goes from ballistic to exponentially suppressed as the value of λ is tuned from the delocalized to localized regime and at the critical point the transport shows anomalous behavior with subdiffusive scaling of the transport coefficient with the system size [23,24].

For nonzero α, i.e., for the GAAH model, the system possesses a single-particle mobility edge which can be obtained analytically, $E = 2\,\mathrm{sgn}(\lambda)(1 - |\lambda|)/\alpha$ [4], where E corresponds to a single-particle energy eigenvalue. In this case, all the single-particle eigenstates with energy less than E are extended/delocalized while those states with energy higher than E are localized. Hence, when E falls within the spectrum, it is a mobility edge.

In Eq. (1), $H_B = H_L + H_R$ represents the Hamiltonian for the left and the right reservoirs. For this study, we model these reservoirs as a one-dimensional (1D) tight-binding ordered semi-infinite chain with Hamiltonian,

$$H_L = \epsilon_0 \sum_k a_k^\dagger a_k + t_0 \sum_k a_{k+1}^\dagger a_k + \text{H.c.}, \tag{4}$$

$$H_R = \epsilon_0 \sum_k b_k^\dagger b_k + t_0 \sum_i b_{k+1}^\dagger b_k + \text{H.c.}, \tag{5}$$

with a_k and b_k corresponding to the annihilation operators of the k th sites for left and right baths, respectively. For simplicity, we choose the same on-site (ϵ_0) and the same hopping parameter (t_0) for both baths. The term $H_{SB} = H_{SL} + H_{SR}$ represents the coupling between the system and the baths and is responsible for the charge transfer across the system. It is specified by

$$H_{SL} = \gamma_L a_1^\dagger c_1 + \text{H.c.}, \tag{6}$$

$$H_{SR} = \gamma_R b_1^\dagger c_N + \text{H.c.}, \tag{7}$$

where the left (right) bath is coupled to the first (N th) site of the quasiperiodic lattice chain with coupling strength γ_L (γ_R).

As mentioned before, the dephasing and dissipation effects within the central lattice chain can be modeled phenomenologically by connecting local reservoirs (probes) at each lattice site. As is done for the left and the right reservoirs, for this study, we model each probe also as a 1D tight-binding ordered semi-infinite chain. The total Hamiltonian for the probes is given as $H_P = \sum_{i=1}^N H_P^i$ with each probe Hamiltonian given by

$$H_P^i = \sum_j [\epsilon_0 d_{ij}^\dagger d_{ij} + t_0 d_{ij+1}^\dagger d_{ij} + \text{H.c.}]. \tag{8}$$

Correspondingly, the coupling Hamiltonian between the i th probe and the central system is given as

$$H_{PS}^i = \gamma c_i^\dagger d_{i1} + \text{H.c.}, \tag{9}$$

where the first site of each probe is coupled to the i th site of the central system with coupling strength γ, which is chosen to be the same for all the probes (see Fig. 1).

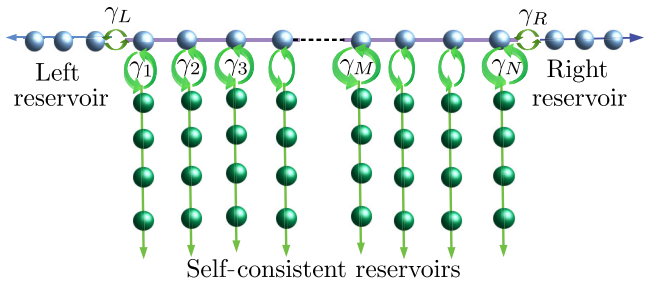

FIG. 1. Schematic of a one-dimensional lattice chain where the first and the last sites of the chain are connected to the left and the right reservoirs, respectively, These reservoirs have different chemical potentials that induce current in the chain. In addition, each lattice site is attached to a local reservoir which we refer to here as the Büttiker probe. The probes, left and right reservoirs, are all modeled as 1D ordered semi-infinite tight-binding chains.

B. Theory

We employ the nonequilibrium Green's function (NEGF) approach [58–63] to investigate end-to-end transport through the central quasiperiodic chain. In the presence of the two baths at the ends and the Büttiker probes, one can obtain the retarded Green's function for the central system as

$$\mathcal{G}^r(\epsilon) = \left[\epsilon I - H_C - \Sigma_L^r(\epsilon) - \Sigma_R^r(\epsilon) - \sum_{i=1}^{N} \Sigma_{P,i}^r(\epsilon)\right]^{-1}, \tag{10}$$

where I is the $N \times N$ identity matrix with N being the number of lattice sites of the central system and is also equal to the total number of probes attached to the central lattice. H_C represents the $N \times N$ single-particle Hamiltonian corresponding to H_S. $\Sigma_\alpha^r(\epsilon)$, $\alpha = L, R, P$, is the self-energy associated with the α th bath. Note that the effects of the baths, including the probes, are additive in the self-energy. Since we have chosen the baths and the Büttiker probes as semi-infinite ordered tight-binding chains, the self-energies in this case can be obtained analytically and given by [64]

$$\Sigma_\alpha^r(\epsilon) = \frac{\gamma_\alpha^2}{2t_0^2}\left[\epsilon - i\sqrt{4t_0^2 - \epsilon^2}\right], \quad \alpha = L, R, P. \tag{11}$$

where $\epsilon_0 = 0$, and $\gamma_P = \gamma$. Before we proceed further, let us fix some notations. We identify the index n with the probe terminals, ν to identify the left and the right reservoirs, and use index α to count all the leads. Since the entire setup is fully quadratic, the average charge current in the steady state flowing out of the ν th reservoir is given by the famous Landauer-Büttiker formula [61]

$$I_\nu = \frac{e}{2\pi}\sum_\alpha \int_{-\infty}^{\infty} d\epsilon\, \mathcal{T}_{\nu\alpha}(\epsilon)[f_\nu(\epsilon) - f_\alpha(\epsilon)], \quad \nu = L, R. \tag{12}$$

Here, $f_\alpha(\epsilon) = (1 + e^{\beta(\epsilon-\mu_\alpha)})^{-1}$ is the Fermi distribution function of the α th terminal with inverse temperature β and chemical potential μ_α. $\mathcal{T}_{\nu\alpha}(\epsilon)$ is the transmission probability for an electron to flow from the ν th terminal to the α th terminal through the quasiperiodic system. The transmission probabilities can be computed using the Green's function of the central system and the self-energy of the baths and expressed as

$$\mathcal{T}_{\nu\alpha}(\epsilon) = \mathrm{Tr}[\Gamma_\nu(\epsilon)\mathcal{G}^r(\epsilon)\Gamma_\alpha(\epsilon)\mathcal{G}^a(\epsilon)], \tag{13}$$

where $\mathcal{G}^a(\epsilon) = [\mathcal{G}^a(\epsilon)]^\dagger$ is the advanced Green's function and $\Gamma_\alpha(\epsilon) = -2\,\mathrm{Im}[\Sigma_\alpha^r(\epsilon)]$.

One can similarly compute the charge current flowing out of the n th probe which is also given by the Landauer-Büttiker formula

$$I_n = \frac{e}{2\pi}\sum_\alpha \int_{-\infty}^{\infty} d\epsilon\, \mathcal{T}_{n\alpha}(\epsilon)[f_n(\epsilon) - f_\alpha(\epsilon)], n = 1, 2, \ldots, N. \tag{14}$$

In what follows, we first analyze the effect on end-to-end conductance properties by considering the local reservoirs as voltage probes and thus set the net charge current flowing out of each probe to zero, i.e., $I_n = 0$ for $n = 1, 2, \ldots, N$ in Eq. (14). Imposing this constraint for each probe allows one to simulate both elastic dephasing and inelastic dissipative processes in the central lattice chain. In Sec. IV, we further extend the above study by considering the local reservoirs as voltage-temperature probes and demand vanishing charge and heat currents from each probe which then allow us to simulate inelastic but nondissipative scattering processes. Under this generic probe setting, we study the thermoelectric heat-to-work conversion properties and the recently obtained tighter bounds on thermoelectric efficiency.

C. Voltage-probe technique in linear-response regime

In this section, we first focus on the voltage-probe technique by considering the temperature of the end reservoirs and the probes to be the same. The different chemical potentials of the two end reservoirs drive a steady-state current in the chain. We impose the zero charge current condition from each probe which in turn fixes the local chemical potential of each probe. We concentrate on the linear-response regime and expand the Fermi-distribution function around the equilibrium chemical potential ϵ_F and inverse temperature β as

$$f_K(\epsilon) = f_{\mathrm{eq}}(\epsilon) - \frac{\partial f_{\mathrm{eq}}(\epsilon)}{\partial\epsilon}(\mu_K - \epsilon_F). \tag{15}$$

The derivative of the Fermi function is also evaluated at ϵ_F. Now putting Eq. (15) in Eq. (14), for each n and setting $I_n = 0, n = 1, 2, \ldots, N$, we receive a set of N linear equations for the chemical potential of each probe n of the form

$$\mu_n = \mu_R + \sum_{j=1}^{N}\left[\mathcal{W}_{nj}^{-1}\int_{-\infty}^{\infty}\mathcal{T}_{jL}(\epsilon)\left(-\frac{\partial f_{\mathrm{eq}}(\epsilon)}{\partial\epsilon}\right)d\epsilon\right] \times (\mu_L - \mu_R), \forall\, n = 1, 2, \ldots, N. \tag{16}$$

Here, $\mathcal{W}$ is an $N \times N$ matrix given as

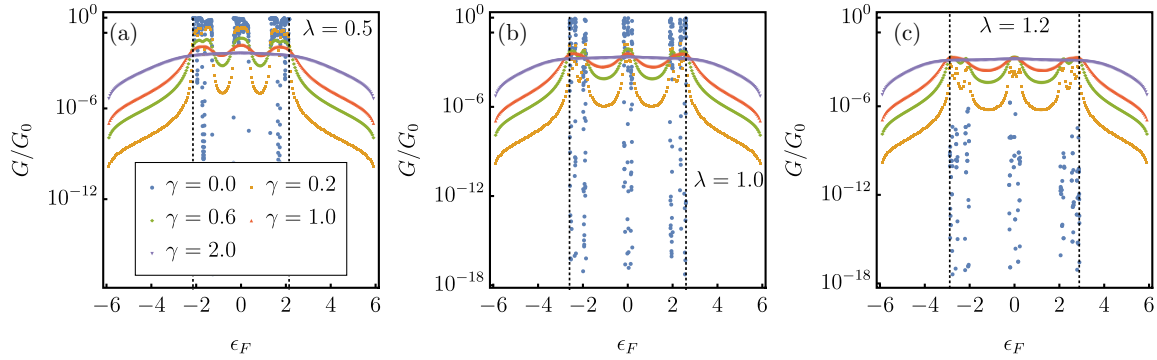

FIG. 2. Plots for zero-temperature conductance in the absence and presence of Büttiker voltage probes for the AAH model in three different transport regimes. In the coherent regime (absence of probes), the AAH model displays delocalized ($\lambda < 1$), critical ($\lambda = 1$), and localized ($\lambda > 1$) phases depending on the strength λ. Here, we display the effect of voltage probes on transport. The vertical dotted lines represent the band edges of the AAH model. Here, the system size is taken as $N = 200$.

$$\mathcal{W} = \begin{pmatrix} \sum_{\alpha\neq 1}\int_{-\infty}^{\infty}\mathcal{T}_{1\alpha}(\epsilon)\left(-\frac{\partial f_{\rm eq}(\epsilon)}{\partial\epsilon}\right)d\epsilon & -\int_{-\infty}^{\infty}\mathcal{T}_{12}(\epsilon)\left(-\frac{\partial f_{\rm eq}(\epsilon}{\partial\epsilon}\right)d\epsilon & -\int_{-\infty}^{\infty}\mathcal{T}_{13}(\epsilon)\left(-\frac{\partial f_{\rm eq}(\epsilon)}{\partial\epsilon}\right)d\epsilon & \cdots \\ -\int_{-\infty}^{\infty}\mathcal{T}_{21}(\epsilon)\left(-\frac{\partial f_{\rm eq}(\epsilon)}{\partial\epsilon}\right)d\epsilon & \sum_{\alpha\neq 2}\int_{-\infty}^{\infty}\mathcal{T}_{2\alpha}(\epsilon)\left(-\frac{\partial f_{\rm eq}(\epsilon)}{\partial\epsilon}\right)d\epsilon & -\int_{-\infty}^{\infty}\mathcal{T}_{23}(\epsilon)\left(-\frac{\partial f_{\rm eq}(\epsilon)}{\partial\epsilon}\right)d\epsilon & \cdots \\ -\int_{-\infty}^{\infty}\mathcal{T}_{31}(\epsilon)\left(-\frac{\partial f_{\rm eq}(\omega)}{\partial\epsilon}\right)d\omega & -\int_{-\infty}^{\infty}\mathcal{T}_{32}(\epsilon)\left(-\frac{\partial f_{\rm eq}(\epsilon)}{\partial\epsilon}\right)d\epsilon & \sum_{\alpha\neq 3}\int_{-\infty}^{\infty}\mathcal{T}_{3\alpha}(\epsilon)\left(-\frac{\partial f_{\rm eq}(\epsilon)}{\partial\epsilon}\right)d\epsilon & \cdots \\ \cdots & \cdots & \cdots & \cdots \end{pmatrix}.$$

Given the local chemical potentials μ_n in Eq. (16), we can compute the electrical conductance G for this setup as, $G = I_R/\Delta V$ with $\Delta V = (\mu_R - \mu_L)/e$ being the applied bias voltage,

$$G = G_0\int_{-\infty}^{\infty}d\epsilon\left(-\frac{\partial f_{\rm eq}(\epsilon)}{\partial\epsilon}\right)\Bigg[\mathcal{T}_{RL}(\epsilon) + \int_{-\infty}^{\infty}d\epsilon'\sum_{nj}\mathcal{T}_{Rn}(\epsilon)\mathcal{W}^{-1}_{nj}\mathcal{T}_{jL}(\epsilon')\left(-\frac{\partial f_{\rm eq}(\epsilon')}{\partial\epsilon'}\right)\Bigg], \tag{17}$$

where $G_0 = e^2/2\pi\hbar$ is the universal quantum electrical conductance. The second term in the above expression reflects the change in the conductance due to the probes by mimicking incoherent scattering processes. In the zero-temperature limit ($\beta \to \infty$) [49], the above equation simplifies drastically as $\frac{\partial f_{\rm eq}(\epsilon)}{\partial\epsilon} = -\delta(\epsilon - \epsilon_F)$, and the conductance can be expressed simply in terms of an effective transmission function $G = G_0\,\mathcal{T}_{\rm eff}(\epsilon_F)$, where

$$\mathcal{T}_{\rm eff}(\epsilon_F) = \mathcal{T}_{RL}(\epsilon_F) + \sum_{nj}\mathcal{T}_{Rn}(\epsilon_F)\mathcal{W}^{-1}_{nj,0}\mathcal{T}_{jL}(\epsilon_F). \tag{18}$$

In the above equation, $\mathcal{W}_{nj,0}$ denotes the matrix elements of $\mathcal{W}$ computed in the zero-temperature limit. Interestingly, for $\beta \to \infty$, the local probes are exactly equivalent to the dephasing probes as the zero-particle current condition from Eq. (14) is now satisfied for each energy.

III. RESULTS: VOLTAGE PROBE

We now present the numerical results for conductance at both zero and finite temperatures. Since the zero-temperature calculation does not require any numerical integration to be performed, one can therefore simulate large system sizes. Here, we report results up to $N = 1597$. Unless otherwise stated, for all the numerical calculations we set $\epsilon_0 = 0$, $t_0 = 3$, $t = 1$, $\gamma_L = \gamma_R = 1$. Note that, to reduce the number of parameters in the problem, we have chosen a spatially uniform situation for the probes by setting $\gamma_n = \gamma$ for all $n = 1, 2, \ldots, N$. We also stress that in the following discussions by coherent transport we imply transport through a quasiperiodic lattice in the absence of the probes ($\gamma_n = 0$).

In Fig. 2 we first display the effects of voltage probes in three different transport regimes of the AAH model corresponding to three different λ values: ballistic [$\lambda = 0.5$, Fig. 2(a)], critical [$\lambda = 1.0$, Fig. 2(b)], and localized [$\lambda = 1.2$, Fig. 2(c)] at zero temperature. In the absence of probes, in all three regimes of the AAH model, there are energy values located within and outside the band of the lattice system (the vertical dotted lines in Fig. 2 represent the band edges of the central lattice chain), at which no significant transport takes place due to the absence of bare energy states of the central system. However, once the voltage probes are attached, the transport properties in all the regimes change significantly. In particular, in the presence of probes, finite transport is induced for all Fermi energies that corresponds to no transport in the coherent case. Moreover, we observe that for these particular energies, the value of conductance increases with increasing system-probe coupling γ. In contrast, for the energy values for which significant transport is already present in the coherent limit, the conductance displays nonmonotonic behavior with increasing γ. Note that, in the localized regime [Fig. 2(c)], as there is essentially no transport for any ϵ_F in the coherent limit, attaching probes always induces finite conductance for all Fermi energies.

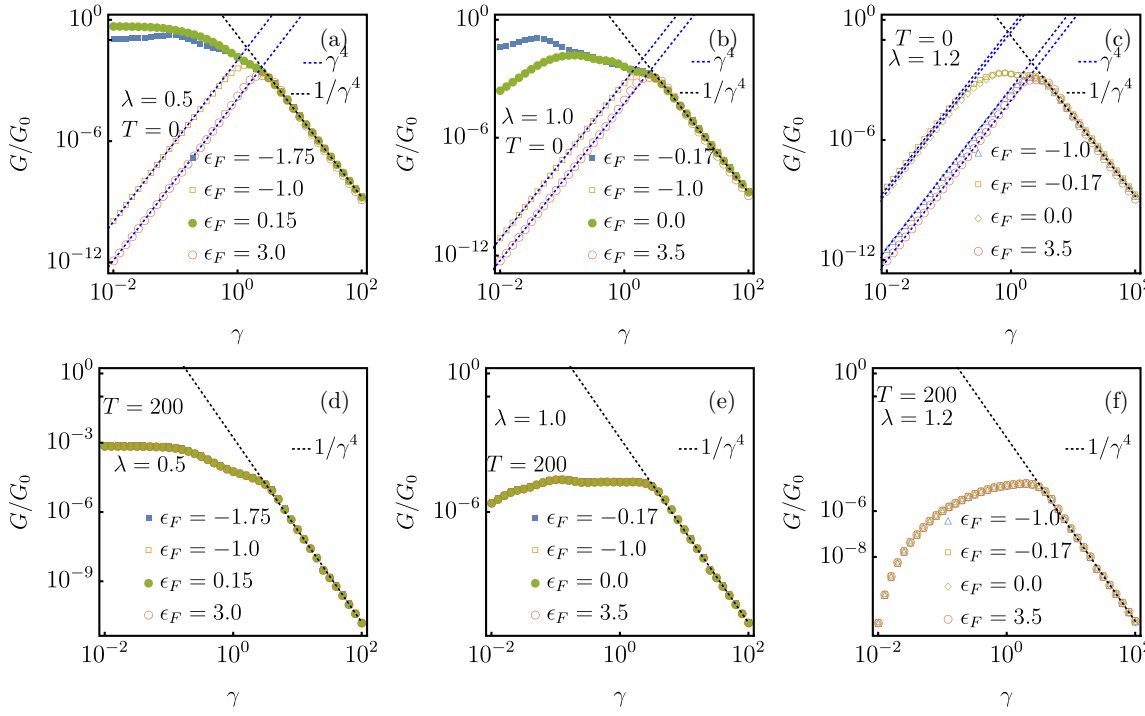

FIG. 3. Plots for zero-temperature conductance as a function of system-probe coupling strength γ in different transport regimes of the AAH model at different Fermi energies. Here, the system size is taken as $N = 200$.

To establish this behavior more explicitly, we choose different ϵ_F's corresponding to no-transport and transport cases in the coherent limit, and plot in Figs. 3(a)–3(c) the zero-temperature conductance as a function of the coupling strength γ. As mentioned before, for no-transport energies, the conductance increases with γ but interestingly as a power law with scaling γ^4 up to a critical value $\gamma_c \sim t, \gamma_L, \gamma_R$. In contrast, no particular scaling is observed for the transport energies where attaching probes may increase or decrease the value of conductance. Note that, for the critical λ [Fig. 3(b)], as the eigenstates of the bare system are not completely delocalized, an increase in conductance is observed even for Fermi energies that corresponds to finite transport. Beyond the critical value of the probe coupling, i.e., $\gamma_c > t, \gamma_L, \gamma_R$, the conductance becomes independent of λ and is equal for all ϵ_F's and more importantly decays as a power law $1/\gamma^4$. Note that this scaling result is different than the one recently predicated following the local Lindblad master equation approach where the analysis was carried out in the infinite-temperature limit with scaling given as $1/\gamma^2$ [34]. In Figs. 3(d)–3(f) we extend these results to the finite-temperature limit. We observed that, at high temperature $T = 200$, the conductance value is the same for all Fermi energies, implying a flat transmission spectrum with ϵ_F. Below γ_c, the contributions to conductance come from all energies that reside within the energy window of width k_BT around ϵ_F and as a result no particular scaling with γ is observed. However, interestingly, for large γ the conductance scaling remains the same as the zero-temperature case. In the Appendix, we provide a detailed proof of this universal scaling for conductance in the strong γ limit.

We next present the scaling of the conductance with the system size N. In Figs. 4(a)–4(c), we display the crossover from various transport regimes in the coherent limit to a diffu-

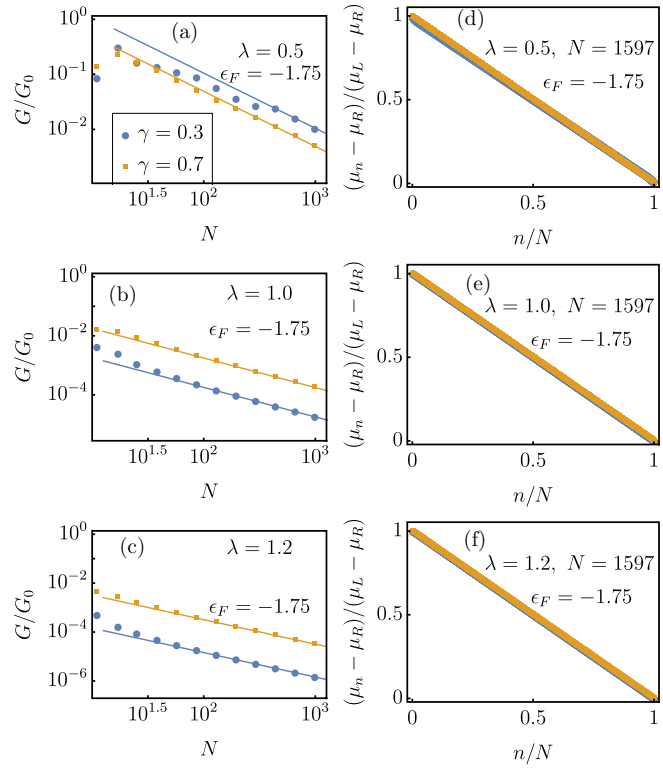

FIG. 4. (a)–(c) show the crossover to the diffusive transport regime from the ballistic ($\lambda = 0.5$), subdiffusive ($\lambda = 1.0$), and exponentially localized ($\lambda = 1.2$) phases, respectively, in the presence of voltage probes at zero temperature. The solid lines represent diffusive $1/N$ scaling. (d)–(f) show the corresponding chemical potential profiles. The linear chemical potential profile ensures that the transport is diffusive. We show results for two different γ values.

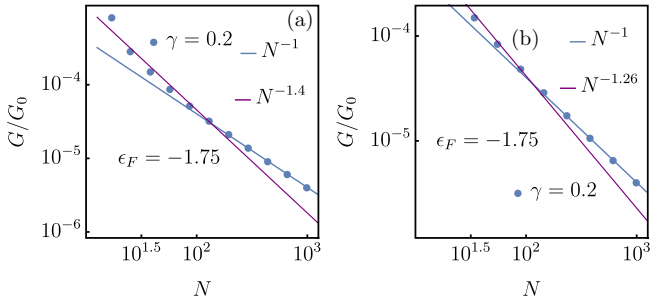

FIG. 5. Crossover from subdiffusive behavior to diffusive behavior for $\gamma = 0.2$ at the critical point ($\lambda = 1$) of the AAH model at zero temperature. Depending on the chosen system size one can see a crossover to N^{-1} from different subdiffusive scalings. In (a), the chosen system sizes do not correspond to Fibonacci numbers, and in (b), the system sizes correspond to Fibonacci numbers.

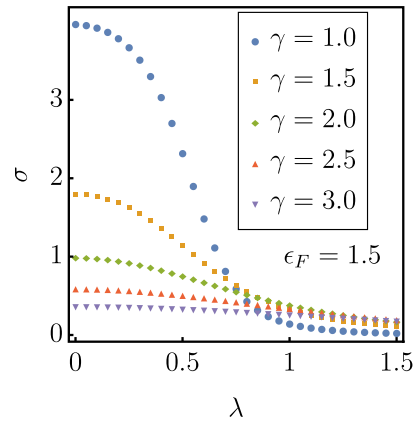

FIG. 7. Plot for electrical conductivity $\sigma = \lim_{N\to\infty} NG$ in the diffusive regime as a function of quasiperiodic lattice strength λ for different values of γ.

sive limit $G \sim N^{-1}$. We note that for a finite system size, with sufficiently strong incoherent effects induced by the probes, the transport eventually becomes diffusive for all λ values. For weak γ, the conductance however displays a crossover from the coherent limit scaling to a diffusive scaling and the corresponding crossover length varies strongly depending on whether the transport is ballistic, subdiffusive, or localized in the coherent regime. As an example, for the same γ value ($\gamma = 0.3$) in the localized case [Fig. 4(c)], the crossover takes place at a small system size $N \sim 30$ compared to the ballistic case $N \sim 200$. This fact corroborates with the predictions in Ref. [34]. For a fixed λ, with increasing γ, the crossover length shrinks and a diffusive scaling sets in. In Figs. 4(d)–4(f), we display the corresponding chemical potential profile in the lattice chain which shows a clear linear behavior in the presence of probes, indicating a diffusive transport.

It is important to note that, in the critical regime of the coherent AAH model ($\gamma = 0$), the conductance can display different subdiffusive scalings depending on the choice of the system size [23,26]. For example, at $\lambda = 1$ (critical regime), if the system size is considered as a Fibonacci number (we have considered here b as the ratio of two Fibonacci numbers), a subdiffusive scaling $N^{-1.26}$ is observed whereas for the case of non-Fibonacci numbers a subdiffusive scaling $N^{-1.4}$ is observed. It is interesting to see that, in the presence of probes, for both cases, a crossover from a subdiffusive to diffusive regime is observed, as shown in Fig. 5. Furthermore, we observe that for all λ, interestingly, the crossover length from coherent to diffusive transport is independent of the temperature, as displayed in Fig. 6.

Since the transport eventually becomes diffusive in the presence of probes, in the diffusive regime we define the electrical conductivity $\sigma = \lim_{N\to\infty} \sigma(N)$ with $\sigma(N) = NG$ being the finite-size conductivity. In Fig. 7, we display σ as a function of λ, the strength of the quasiperiodic potential. The conductivity σ strongly depends on λ with the value monotonically decreasing with increasing λ. This implies that even though the system is in the diffusive regime, the conductivity is still larger in the $\lambda < 1$ regime in comparison to the $\lambda > 1$ regime. However, for large γ, the quasiperiodic nature of the lattice is smeared out by the probe coupling and conductivity becomes essentially insensitive to the value of λ.

We next briefly discuss the results for the generalized AAH, i.e., the GAAH model [see Eq. (3)]. In this case, we observe similar trends in conductance to the one observed for the AAH model. As was done in Fig. 2, in Fig. 8 we plot G as a function of ϵ_F in the presence of a mobility edge. For the chosen parameters in our simulations, all the states above

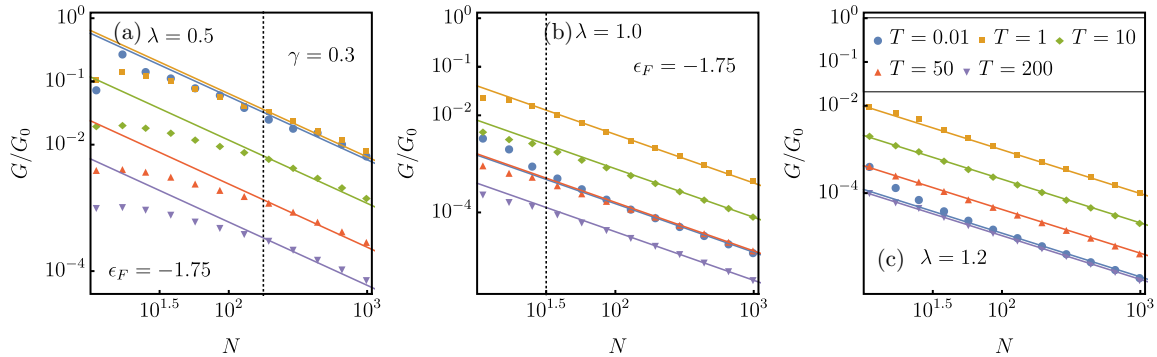

FIG. 6. (a)–(c) show the crossover to the diffusive regime at finite temperatures for probe coupling strength $\gamma = 0.3$. The solid lines represent diffusive $1/N$ scaling. The vertical dotted lines represent the system size after which the diffusive transport sets further, indicating a temperature-independent system-size crossover.

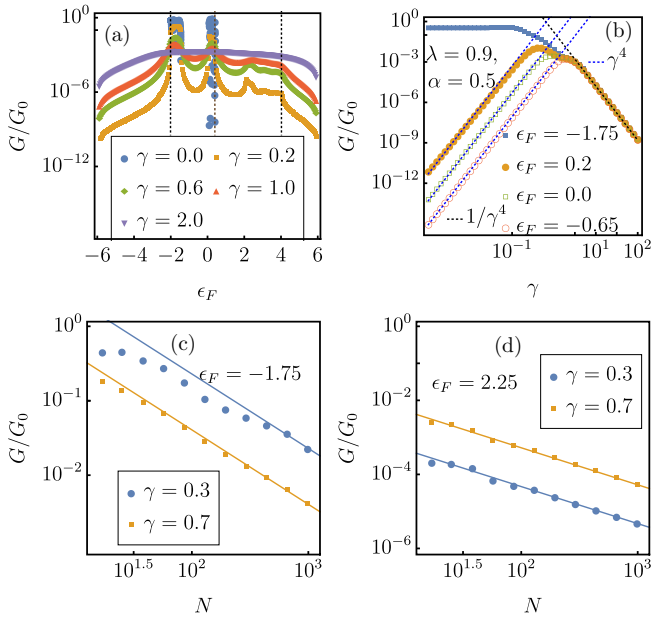

FIG. 8. Results for the GAAH model: (a) displays the effect of probes on transport. The dotted vertical lines at the two ends represent the band edges and the vertical line in the middle represents the mobility edge. (b) displays conductance as a function of γ for different Fermi energies. (c) and (d) show the crossover to the diffusive regime from both no-transport and transport regimes in the presence of probes.

(below) the mobility edge are localized (delocalized). As can be seen in Fig. 8(b), in all the no-transport regimes, due to the coupling with probes, there is an enhancement of G up to a critical $\gamma_c \sim t, \gamma_L, \gamma_R$ with conductance increasing as γ^4 and thus displaying universality. Furthermore, beyond γ_c, similar to the AAH case, the G decreases as $1/\gamma^4$. In Figs. 8(c) and 8(d), we show that for this model also, the transport eventually becomes diffusive at all regimes.

IV. RESULTS: VOLTAGE-TEMPERATURE PROBE TECHNIQUE AND THERMOELECTRIC PERFORMANCE

In this section we extend our study to the voltage-temperature probe that enables us to investigate thermoelectric properties. In this case, the left and right reservoirs are kept at fixed chemical potentials (μ_L, μ_R) and temperatures (T_L, T_R). Next, we impose the voltage-temperature probe conditions of zero particle and heat currents flowing out of each probe and thereby determine the chemical potential and temperature of each probe. Thus, we set

$$I_n = \frac{e}{\hbar}\sum_\alpha \int_{-\infty}^{\infty} d\epsilon \mathcal{T}_{n\alpha}(\epsilon)[f_n(\epsilon) - f_\alpha(\epsilon)] = 0,$$
$$Q_n = \frac{1}{\hbar}\sum_\alpha \int_{-\infty}^{\infty} d\epsilon(\epsilon - \mu_n)\mathcal{T}_{n\alpha}(\epsilon)[f_n(\epsilon) - f_\alpha(\epsilon)] = 0,$$
$$n = 1, 2, \ldots, N \tag{19}$$

Once again, we focus on the linear-response regime and obtain μ_n and T_n for the probes in terms of μ_L, μ_R, T_L, and T_R. Finally, we can write the particle (I_R) and heat currents (Q_R) flowing out from the right bath as

$$\langle I_R\rangle = G\,\Delta V + G\,S\,\Delta T,$$
$$\langle Q_R\rangle = G\,\Pi\Delta V + (K + G\,S\,\Pi)\Delta T, \tag{20}$$

where G is the electrical conductance, K is the thermal conductance, S is the Seebeck coefficient, and Π is the Peltier coefficient. Here, $\Delta V = (\mu_R - \mu_L)/e$ and $\Delta T = T_R - T_L$. All of the above transport coefficients depend on the average temperature $T = (T_L + T_R)/2$ and average chemical potential $\epsilon_F = (\mu_L + \mu_R)/2$. In the presence of the probes, we numerically verified the Onsager's reciprocity relation, given by $\Pi = TS$. Note that in order to compute G, Π, S, and K in the presence of voltage-temperature probes, we first consider $\Delta T = 0$ and extract the transport coefficients G and Π and next consider $\Delta V = 0$ to extract the other two coefficients S and K. Now in order to realize a thermoelectric engine, we set $\mu_L > \mu_R$ and $T_R > T_L$ and demand $\langle I_R\rangle > 0$ and $\langle Q_R\rangle > 0$, i.e., heat absorbed from the hot right bath induces particle current against the chemical potential difference. The average power output is then given as $\langle P\rangle = -\Delta V\,\langle I_R\rangle$, and as a result, the average thermoelectric efficiency of the engine is given by $\langle\eta\rangle = \frac{\langle P\rangle}{\langle Q_R\rangle}$. In the linear-response regime, the maximum thermoelectric efficiency $\langle\eta\rangle_{\max}$ is characterized by a single dimensionless quantity, the thermoelectric figure of merit $ZT = \frac{GS^2}{K}T$, and is given as

$$\langle\eta\rangle_{\max} = \eta_C \frac{\sqrt{ZT+1} - 1}{\sqrt{ZT+1} + 1}, \tag{21}$$

where $\eta_C = \Delta T/T$ is the Carnot efficiency in the linear-response regime. In Figs. 9(a)–9(f), we display the behavior of various transport coefficients and ZT for the AAH model as a function of γ, for different values of λ. As the electrical conductance G, the thermal conductance K also shows a similar scaling $1/\gamma^4$ at strong probe coupling in all regimes. The Seebeck coefficient, however, does not display any such scaling. Starting in the $\lambda < 1$ regime, the values for both G and K are always lower than that in the coherent limit, whereas probe-induced enhancement can be seen in both $\lambda = 1$ and $\lambda > 1$ regimes [Figs. 9(c)–9(e)]. As a result, ZT decays with increasing γ in the $\lambda < 1$ regime but in the other two regimes an enhancement in the ZT value, compared to the coherent limit, is seen for some values of γ. Note that the overall value of ZT, however, always remains higher for $\lambda < 1$ in comparison to the other two regimes. For large γ, all three regimes converge to the same ZT value.

We next move on to analyze two recently obtained universal bounds [56,57] for the mean efficiency in the context of our thermoelectric engines. Interestingly, these universal bounds are found to be tighter than the seminal Carnot bound and are written in terms of the current fluctuations. One of the bounds emerges from the recently discovered thermodynamic uncertainty relations (TURs) [57,65,66] which are trade-off relations between power, efficiency, and power fluctuation. In the context of a thermoelectric engine, operating in the linear-response regime, following the TURs we obtain the bound on mean efficiency as

$$\langle\eta\rangle \leqslant \frac{\mu_L - \mu_R}{eT}\frac{1}{S} \leqslant \eta_c. \tag{22}$$

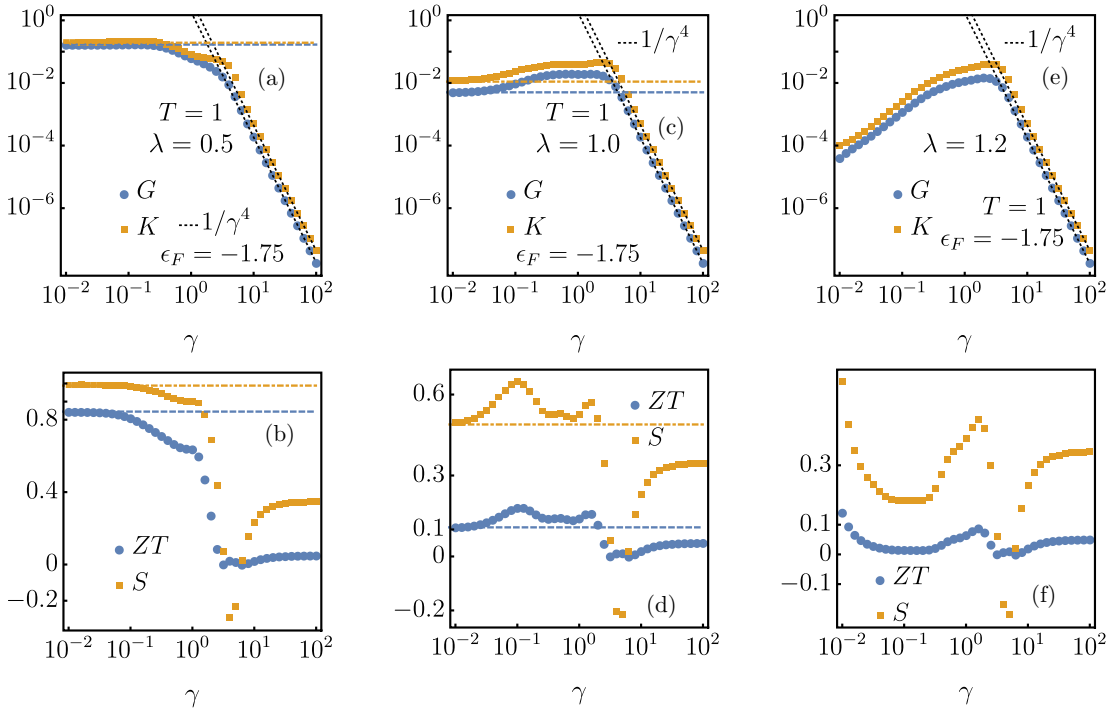

FIG. 9. (a)–(f) display the various transport coefficients and the ZT for the AAH model as a function of probe coupling strength γ in the presence of voltage-temperature probes. The horizontal lines in (a)–(d) represent the values of transport coefficients in the coherent limit ($\gamma = 0$).

Note that the Seebeck coefficient S is always positive in the engine regime.

Very recently, another tighter bound on the engine's efficiency was obtained in Refs. [56,67] by identifying the input and output currents and imposing conditions on the direction of these currents such that the thermoelectric setup operates as an engine. Following this bound, we receive

$$\langle \eta \rangle \leqslant \frac{\mu_L - \mu_R}{eT} \frac{1}{S} \sqrt{\frac{ZT}{ZT+1}} \leqslant \eta_c. \tag{23}$$

Since $ZT > 0$, we arrive at an important conclusion that the bound predicted by Eq. (23) is always tighter than the one given in Eq. (22). In Fig. 10 we assess the bounds in Eq. (23) for the AAH model in the presence of the probes as a function of γ and for different λ values. Denoting $\eta_B = \frac{\mu_L - \mu_R}{eT} \frac{1}{S} \sqrt{\frac{ZT}{ZT+1}}$, we observe that $\langle \eta \rangle - \eta_B$ and $\eta_B - \eta_C$ are always negative in the parameter regimes considered here. Thus, we find that the bounds in Eqs. (22) and (23), obtained in the linear-response regime, are valid even in the presence of the probes.

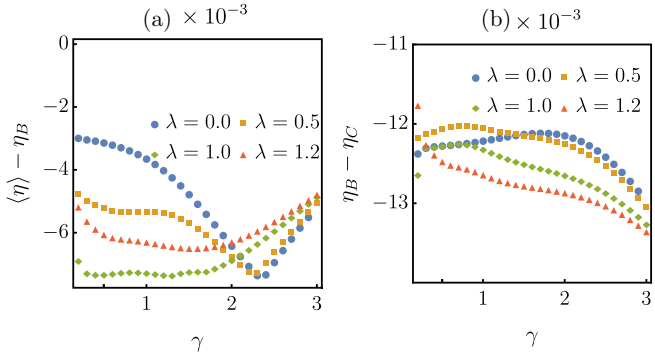

FIG. 10. Plots for (a) tighter bound on mean efficiency, i.e., $\langle \eta \rangle - \eta_B$, and (b) the bound $\eta_B - \eta_C$ as functions of γ for different values of λ. The parameters are $N = 34$, $T = 1$, $\Delta T = 0.2$, $\mu = -1.75$, $\mu_R - \mu_L = -0.001$.

V. SUMMARY

In summary, we have investigated the transport properties in quasiperiodic systems following the Büttiker probe approach by implementing both voltage and voltage-temperature probe conditions. Within the voltage-probe framework, in the strong probe coupling limit, we observed a power-law decay of electrical conductance with the probe coupling strength. This behavior is in fact independent of the Fermi energy, the nature of the on-site potential, and the temperature. Moreover, within the voltage-temperature probe scheme, in addition to the electrical conductance, the thermal conductance also displays the same power-law decay with the probe coupling. In this sense, the power-law decay of transport coefficients is universal. Importantly, this power-law scaling observed here turns out to be different from what was reported in a recent work following the local Lindblad master equation approach [34]. This further pinpoints that the two different approaches, namely NEGF and the local Lindblad master equation, effectively mimic different underlying scattering processes. In the presence of a voltage probe we also observed that the conductance of all the exponentially decaying regimes (namely the localized regimes of the AAH model, above the mobility edge of the GAAH model, outside the band edges of

the central lattice system, and the band-gap regimes) initially gets enhanced with a particular power-law scaling with the probe coupling strength at zero temperature. Thus, we have reported here the environment-assisted transport with a particular scaling for the "no-transport" regimes at zero temperature. With finite-temperature and voltage-temperature probes, no particular scaling is observed in the no-transport regimes. For sufficiently strong coupling, the transport eventually becomes diffusive in all regimes of the original model. However, with finite but small probe coupling, a crossover from coherent transport to diffusive transport can be observed. Such a crossover length is insensitive to the temperature but depends crucially on the transport regime of the original model. We also investigated the thermoelectric properties by incorporating voltage-temperature probes and further assessed, in the presence of probes, the validity of two recently obtained tighter bounds on efficiency, and also showed that the bound predicted from the TUR is always looser than the other bound.

ACKNOWLEDGMENTS

The authors would like to acknowledge Archak Purkayastha for numerous useful discussions. M.S. acknowledges funding from National Postdoctoral Fellowship Scheme (NPDF), SERB file No. PDF/2020/000992. B.P.V. is supported by a Department of Science & Technology Science and Engineering Research Board (India) Start-up Research Grant No. SRG/2019/001585. B.K.A. acknowledges the MATRICS Grant No. MTR/2020/000472 from SERB, Government of India and the Shastri Indo-Canadian Institute for providing financial support for this research work in the form of a Shastri Institutional Collaborative Research Grant (SICRG).

APPENDIX: PROOF OF THE UNIVERSAL POWER-LAW DECAY $\frac{1}{N\gamma^4}$ FOR THE CONDUCTANCE G IN THE STRONG γ LIMIT

In this Appendix we provide a rigorous proof for the universal power-law decay of the conductance with the system size and the probe coupling strength γ in the strong probe coupling limit and at zero temperature. We show that in this limit, the conductance takes the form $G \sim \frac{1}{N\gamma^4}$, which further indicates a diffusive behavior, as expected in the strong probe coupling limit. Now in order to arrive at this result, we need to compute the effective transmission, as given in Eq. (18). We therefore first compute the retarded Green's function components in the strong γ limit followed by the calculation of the $\mathcal{W}$ matrix.

1. Analytical calculation of the retarded Green's function $\mathcal{G}^r_{ij}$ in the strong γ limit

In general, for any nearest-neighbor tight-binding lattice with on-site energy ϵ_i and hopping strength t, we can write down the the retarded Green's function $\mathcal{G}^r$ as

$$\mathcal{G}^r = \mathcal{M}^{-1} = \frac{1}{t}\begin{pmatrix} a_{11} & 1 & 0 & 0 & \cdots \\ 1 & a_{22} & 1 & 0 & \cdots \\ 0 & 1 & a_{33} & 1 & \cdots \\ \cdots & \cdots & \cdots & \cdots & \\ 0 & 0 & 0 & 1 & a_{NN} \end{pmatrix}^{-1}.$$

Note that the first and the last site of the lattice are coupled to the left and the right reservoir, respectively, and also to the probes, whereas all other sites are only connected to the probes. As a result, we can write down the matrix elements as

$$\begin{aligned} a_{11} &= \frac{1}{t}\left[\epsilon - \epsilon_1 - \frac{(\gamma_L^2+\gamma_P^2)}{2t_0^2}\left[\epsilon - i\sqrt{4t_0^2-\epsilon^2}\right]\right], \\ a_{2i} &= \frac{1}{t}\left[\epsilon - \epsilon_i - \frac{\gamma_P^2}{2t_0^2}\left[\epsilon - i\sqrt{4t_0^2-\epsilon^2}\right]\right], i = 2,\ldots,N-1, \\ a_{NN} &= \frac{1}{t}\left[\epsilon - \epsilon_N - \frac{(\gamma_R^2+\gamma_P^2)}{2t_0^2}\left[\epsilon - i\sqrt{4t_0^2-\epsilon^2}\right]\right], \end{aligned} \tag{A1}$$

where we used the self-energy expression $\Sigma^r_\alpha(\epsilon) = \frac{\gamma_\alpha^2}{2t_0^2}[\epsilon - i\sqrt{4t_0^2-\epsilon^2}]$, $\alpha = L, R, P$. Now, as done in our numerics, we assume a homogeneous probe coupling strength, i.e., $\gamma_P = \gamma$. In the limit of strong coupling $\gamma \gg t_0, \epsilon_i, \epsilon, \gamma_L, \gamma_R$, all the diagonal elements of the above matrix are the same and given as $a_{ii} = -i\frac{\gamma^2}{t\,t_0}$, $i = 1, 2, \ldots, N$. Note that to arrive at this result we also assumed t_0 to be larger than the system band energies. In what follows, since we are only interested in the scaling with γ^2, we therefore only keep track of these parameters and suppress all the other parameters of the setup.

The inverse of this tridiagonal matrix can be computed easily following a transfer matrix approach [50]. It is to check that

$$\mathcal{G}^r_{ij} = (-1)^{i+j}\frac{\Delta_{1,i-1}\Delta_{N-j,N}}{\Delta_{1,N}}, \quad j > i, \tag{A2}$$

and $\mathcal{G}^r_{ij} = \mathcal{G}^r_{ji}$ for $i > j$. Here, $\Delta_{i,j}$ is the determinant of the submatrix starting with the i th row and column and ending with the j th row and column. The determinant of each of this submatrix is related to the product of transfer matrices $T_a = \left(\begin{smallmatrix} -i\gamma^2 & -1 \\ 1 & 0 \end{smallmatrix}\right)$. With this in hand, it is easy to check that $\mathcal{G}^r_{ij} \sim |\lambda_+|^{-|i-j|-1}$, where λ_+ is the largest eigenvalue of the 2×2 transfer matrix T_a. In this strong γ limit, $|\lambda_+| \sim \gamma^2$. Thus, $\mathcal{G}^r_{ij} \sim \gamma^{-2(|j-i|+1)}$. Similarly, $\mathcal{G}_{iN} \sim \gamma^{-2(|N-i|+1)}$ and $\mathcal{G}^r_{1i} \sim \gamma^{-2i}$. As a result, we can write down the transmission probabilities as $T_{ij} = \gamma^4|\mathcal{G}_{ij}|^2 \sim \gamma^{-4|j-i|}$, $T_{iR} = T_{Ri} = \gamma^2|\mathcal{G}^r_{iN}|^2 \sim \gamma^{-2}\gamma^{-4|N-i|}$, and $T_{iL} = T_{Li} = \gamma^2|\mathcal{G}_{i1}|^2 \sim \gamma^{-2}\gamma^{-4|i-1|}$.

2. Analytical form of the $\mathcal{W}$ matrix and its inverse in the strong γ limit

With the above result for $\mathcal{G}_{ij}$, we now construct the $\mathcal{W}$ matrix in the strong γ regime. Along the diagonal of the $\mathcal{W}$ matrix, the first and last matrix elements contain the dominant contribution as $1/\gamma^2$ which appears from the T_{1L} and T_{NR} terms, respectively. The other diagonal elements depend on γ as $1/\gamma^4$. The off-diagonal elements of $\mathcal{W}_{ij}$ depend on γ as $\gamma^{-4|i-j|}$. We therefore consider only the first neighbors of the diagonal entries, i.e., for $|i-j| = 1$, which gives the

dominant contribution as $1/\gamma^4$ and all the other off-diagonal terms can be neglected. Thus, $\mathcal{W}$ reduces to a tridiagonal matrix in this strong γ limit, given as

$$\mathcal{W} = \begin{pmatrix} 1/\gamma^2 & -1/\gamma^4 & 0 & 0 & \cdots \\ -1/\gamma^4 & 2/\gamma^4 & -1/\gamma^4 & 0 & \cdots \\ 0 & -1/\gamma^4 & 2/\gamma^4 & -1/\gamma^4 & \cdots \\ \cdots & \cdots & \cdots & \cdots & \\ 0 & 0 & 0 & -1/\gamma^4 & 1/\gamma^2 \end{pmatrix}.$$

Now, to check the leading-order behavior of γ in the conductance following the expression for effective transmission [Eq. (18)], the most dominant contribution comes from $T_{NR} \sim 1/\gamma^2$ (independent of N) and $T_{1L} \sim 1/\gamma^2$ (independent of N). Thus, we need to calculate the $\mathcal{W}^{-1}_{N1}$ element to see the leading-order behavior, given as $\mathcal{W}^{-1}_{N1} = 1/\Delta_{1,N}[\mathcal{W}]$. The determinant $\Delta_{1,N}[\mathcal{W}]$ can be once again computed following the transfer matrix approach,

$$\begin{pmatrix} \Delta_{1,N}[\mathcal{W}] \\ \Delta_{1,N-1}[\mathcal{W}] \end{pmatrix} = \frac{1}{\gamma^4}\begin{pmatrix} \gamma^2 & -1 \\ 1 & 0 \end{pmatrix}\begin{pmatrix} 2 & -1 \\ 1 & 0 \end{pmatrix}^{N-2}\begin{pmatrix} \gamma^2 & -1 \\ 1 & 0 \end{pmatrix} \times \begin{pmatrix} 1 \\ 0 \end{pmatrix}. \tag{A3}$$

Interestingly, the matrix $\left(\begin{smallmatrix} 2 & -1 \\ 1 & 0 \end{smallmatrix}\right)$ is nondiagonalizable. One can however write it as the Jordan normal form $J = \left(\begin{smallmatrix} 1 & 1 \\ 0 & 1 \end{smallmatrix}\right)$ using a transformation S. Thus, we can rewrite the matrix equation as

$$\begin{aligned} \begin{pmatrix} \Delta_{1,N}[\mathcal{W}] \\ \Delta_{1,N-1}[\mathcal{W}] \end{pmatrix} &= \frac{1}{\gamma^4}\begin{pmatrix} \gamma^2 & -1 \\ 1 & 0 \end{pmatrix} S J^{N-2} S^{-1} \begin{pmatrix} \gamma^2 \\ 1 \end{pmatrix} \\ &= \frac{1}{\gamma^4}\begin{pmatrix} \gamma^2 & -1 \\ 1 & 0 \end{pmatrix} S \begin{pmatrix} 1 & N-2 \\ 0 & 1 \end{pmatrix} S^{-1} \begin{pmatrix} \gamma^2 \\ 1 \end{pmatrix}, \end{aligned} \tag{A4}$$

with $S = \left(\begin{smallmatrix} i & 0 \\ i & -i \end{smallmatrix}\right)$. Using this, $\Delta_{1,N}[\mathcal{W}] \sim \frac{N}{\gamma^4}(A\gamma^4 + B\gamma^2 + C) + D$ with constant A, B, C, and D. Thus with large γ, $\mathcal{W}^{-1}_{N1} \sim 1/(AN + D)$ and is independent of γ. Thus, in the second term of Eq. (18), we obtain $G \propto T_{\text{eff}} \approx T_{RN}\mathcal{W}^{-1}_{N1}T_{1L} \sim \frac{1}{N\gamma^4}$, which gives us the desired scaling for conductance. The derived result also shows that in the strong γ regime the conductance scales as $1/N$, indicating a diffusive behavior.

[1] S. Aubry and G. André, Ann. Isr. Phys. Soc. **3**, 133 (1980).
[2] P. G. Harper, Proc. Phys. Soc., London, Sect. A **68**, 874 (1955).
[3] S. Ganeshan, K. Sun, and S. Das Sarma, Phys. Rev. Lett. **110**, 180403 (2013).
[4] S. Ganeshan, J. H. Pixley, and S. Das Sarma, Phys. Rev. Lett. **114**, 146601 (2015).
[5] S. Ostlund, R. Pandit, D. Rand, H. J. Schellnhuber, and E. D. Siggia, Phys. Rev. Lett. **50**, 1873 (1983).
[6] J. Sutradhar, S. Mukerjee, R. Pandit, and S. Banerjee, Phys. Rev. B **99**, 224204 (2019).
[7] R. Modak and S. Mukerjee, Phys. Rev. Lett. **115**, 230401 (2015).
[8] J.-y. Choi, S. Hild, J. Zeiher, P. Schauß, A. Rubio-Abadal, T. Yefsah, V. Khemani, D. A. Huse, I. Bloch, and C. Gross, Science **352**, 1547 (2016).
[9] Y. E. Kraus, Y. Lahini, Z. Ringel, M. Verbin, and O. Zilberberg, Phys. Rev. Lett. **109**, 106402 (2012).
[10] M. Verbin, O. Zilberberg, Y. E. Kraus, Y. Lahini, and Y. Silberberg, Phys. Rev. Lett. **110**, 076403 (2013).
[11] F. A. An, K. Padavić, E. J. Meier, S. Hegde, S. Ganeshan, J. H. Pixley, S. Vishveshwara, and B. Gadway, Phys. Rev. Lett. **126**, 040603 (2021).
[12] H. P. Lüschen, S. Scherg, T. Kohlert, M. Schreiber, P. Bordia, X. Li, S. Das Sarma, and I. Bloch, Phys. Rev. Lett. **120**, 160404 (2018).
[13] H. P. Lüschen, P. Bordia, S. S. Hodgman, M. Schreiber, S. Sarkar, A. J. Daley, M. H. Fischer, E. Altman, I. Bloch, and U. Schneider, Phys. Rev. X **7**, 011034 (2017).
[14] M. Atala, M. Aidelsburger, M. Lohse, J. T. Barreiro, B. Paredes, and I. Bloch, Nat. Phys. **10**, 588 (2014).
[15] Y. Lahini, R. Pugatch, F. Pozzi, M. Sorel, R. Morandotti, N. Davidson, and Y. Silberberg, Phys. Rev. Lett. **103**, 013901 (2009).
[16] T. Kohlert, S. Scherg, X. Li, H. P. Lüschen, S. Das Sarma, I. Bloch, and M. Aidelsburger, Phys. Rev. Lett. **122**, 170403 (2019).
[17] V. Balachandran, S. R. Clark, J. Goold, and D. Poletti, Phys. Rev. Lett. **123**, 020603 (2019).
[18] C. Chiaracane, M. T. Mitchison, A. Purkayastha, G. Haack, and J. Goold, Phys. Rev. Research **2**, 013093 (2020).
[19] M. Saha and S. K. Maiti, J. Phys. D: Appl. Phys. **52**, 465304 (2019).
[20] M. Saha and S. K. Maiti, Phys. E (Amsterdam, Neth.) **93**, 275 (2017).
[21] M. Kohmoto, B. Sutherland, and C. Tang, Phys. Rev. B **35**, 1020 (1987).
[22] A. Purkayastha, A. Dhar, and M. Kulkarni, Phys. Rev. B **96**, 180204(R) (2017).
[23] A. Purkayastha, S. Sanyal, A. Dhar, and M. Kulkarni, Phys. Rev. B **97**, 174206 (2018).
[24] M. Saha, S. K. Maiti, and A. Purkayastha, Phys. Rev. B **100**, 174201 (2019).
[25] M. Saha, B. K. Agarwalla, and B. P. Venkatesh, Phys. Rev. A **103**, 023330 (2021).
[26] V. K. Varma, C. de Mulatier, and M. Žnidarič, Phys. Rev. E **96**, 032130 (2017).
[27] M. Žnidarič and M. Ljubotina, Proc. Natl. Acad. Sci. USA **115**, 4595 (2018).
[28] V. K. Varma and M. Žnidarič, Phys. Rev. B **100**, 085105 (2019).
[29] F. S. Lozano-Negro, P. R. Zangara, and H. M. Pastawski, Chaos, Solitons Fractals **150**, 111175 (2021).
[30] M. Žnidarič and M. Horvat, Eur. Phys. J. B **86**, 67 (2013).
[31] M. V. Medvedyeva, T Prosen, and M. Žnidarič, Phys. Rev. B **93**, 094205 (2016).
[32] M. Žnidarič, J. J. Mendoza-Arenas, S. R. Clark, and J. Goold, Ann. Phys. 529, 1600298 (2017).

[33] M. Žnidarič, Phys. Rev. B **97**, 214202 (2018).
[34] A. M. Lacerda, J. Goold, and G. T. Landi, Phys. Rev. B **104**, 174203 (2021).
[35] D. Dwiputra and F. P. Zen, Phys. Rev. A **104**, 022205 (2021).
[36] C. Chiaracane, A. Purkayastha, M. T. Mitchison, and J. Goold, Phys. Rev. B **105**, 134203 (2022).
[37] E. Zerah-Harush and Y. Dubi, Phys. Rev. Research **2**, 023294 (2020).
[38] X. Turkeshi and M. Schiró, Phys. Rev. B **104**, 144301 (2021).
[39] A. Lahiri, K. Gharavi, J. Baugh, and B. Muralidharan, Phys. Rev. B **98**, 125417 (2018).
[40] C. J. Cattena, R. A. Bustos-Marún, and H. M. Pastawski, Phys. Rev. B **82**, 144201 (2010).
[41] D. Nozaki, C. Gomes da Rocha, H. M. Pastawski, and G. Cuniberti, Phys. Rev. B **85**, 155327 (2012).
[42] J. Maassen, F. Zahid, and H. Guo, Phys. Rev. B **80**, 125423 (2009).
[43] D. Nozaki, Y. Girard, and K. Yoshizawa, J. Phys. Chem. C **112**, 17408 (2008).
[44] M. Kilgour and D. Segal, J. Chem. Phys. **144**, 124107 (2016).
[45] M. Kilgour and D. Segal, J. Chem. Phys. **143**, 024111 (2015).
[46] R. Korol, M. Kilgour, and D. Segal, Comput. Phys. Commun. **224**, 396 (2018).
[47] M. Bandyopadhyay and D. Segal, Phys. Rev. E **84**, 011151 (2011).
[48] S. Bedkihal, M. Bandyopadhyay, and D. Segal, Eur. Phys. J. B **86**, 506 (2013).
[49] J. L. D'Amato and H. M. Pastawski, Phys. Rev. B **41**, 7411 (1990).
[50] D. Roy, J. Phys.: Condens. Matter **20**, 025206 (2008).
[51] D. Roy and A. Dhar, Phys. Rev. B **75**, 195110 (2007).
[52] M. Büttiker, Phys. Rev. B **32**, 1846 (1985).
[53] M. Büttiker, Phys. Rev. B **33**, 3020 (1986).
[54] S. Pilgram, P. Samuelsson, H. Förster, and M. Büttiker, Phys. Rev. Lett. **97**, 066801 (2006).
[55] H. Förster, P. Samuelsson, S. Pilgram, and M. Büttiker, Phys. Rev. B **75**, 035340 (2007).
[56] S. Saryal, M. Gerry, I. Khait, D. Segal, and B. K. Agarwalla, Phys. Rev. Lett. **127**, 190603 (2021).
[57] P. Pietzonka and U. Seifert, Phys. Rev. Lett. **120**, 190602 (2018).
[58] J. Schwinger, J. Math. Phys. **2**, 407 (1961).
[59] L. V. Keldysh, Zh. Eksp. Teor. Fiz. **47**, 1515 (1964) [Sov. Phys. JETP **20**, 1018 (1965)].
[60] J. Rammer and H. Smith, Rev. Mod. Phys. **58**, 323 (1986).
[61] H. Haug and A. Jauho, *Quantum Kinetics in Transport and Optics of Semiconductors* (Springer, New York, 2008).
[62] J.-S. Wang, B. K. Agarwalla, H. Li, and J. Thingna, Front. Phys. **9**, 673 (2014).
[63] Y. Meir and N. S. Wingreen, Phys. Rev. Lett. **68**, 2512 (1992).
[64] A. Dhar and D. Sen, Phys. Rev. B **73**, 085119 (2006).
[65] A. C. Barato and U. Seifert, Phys. Rev. Lett. **114**, 158101 (2015).
[66] T. R. Gingrich, J. M. Horowitz, N. Perunov, and J. L. England, Phys. Rev. Lett. **116**, 120601 (2016).
[67] S. Mohanta, S. Saryal, and B. K. Agarwalla, Phys. Rev. E **105**, 034127 (2022).